Am J Cancer Res 2022;12(8):3760-3779
www.ajcr.us /ISSN:2156-6976/ajcr0143878

Original Article

TXNIP inhibits the progression of osteosarcoma through DDIT4-mediated mTORC1 suppression

Yuhao Yuan[1], Qing Liu[1], Ziyi Wu[1], Wei Zhong[1], Zili Lin[1], Wei Luo[1,2]

[1]*Department of Orthopaedics, Xiangya Hospital, Central South University, Changsha, Hunan, P. R. China;* [2]*National Clinical Research Center for Geriatric Disorders, Xiangya Hospital, Changsha, Hunan, P. R. China*

Received May 3, 2022; Accepted July 12, 2022; Epub August 15, 2022; Published August 30, 2022

Abstract: Osteosarcoma (OS) is the most common primary malignant bone tumor in adolescents and children. The pathogenesis of this disease is complex and the mechanisms involved have not been fully elucidated. Thioredoxin-interacting protein (TXNIP), as a member of the α-rhodopsin inhibitory protein family, can combine with thioredoxin to inhibit its antioxidant function. This process inhibits glucose absorption and metabolic rearrangement necessary for the regulation of cellular growth. In recent years, TXNIP has emerged as a new candidate target for tumors. However, the biological function and role of TXNIP in OS remains unclear. This study confirmed the low expression of TXNIP in OS tissues and cells, which was significantly related to the poor survival rate and clinical characteristics of patients with OS. Various cell phenotype experiments have shown that TXNIP inhibits the proliferation, migration, and invasion of OS cells, and promotes their apoptosis. Further studies found that the tumor suppressor effect of TXNIP was mediated by upregulating DNA damage-inducible transcript 4 (DDIT4) and inhibiting the phosphorylation of mechanistic target of rapamycin complex 1 (mTORC1) downstream substrate S6. Based on the above, our study explored the key role of TXNIP/DDIT4/mTORC1 suppression as a regulatory axis in the progression of OS, and laid the foundation for precise targeted therapy for OS.

Keywords: Osteosarcoma, TXNIP, DDIT4, mTORC1, tumor progression

Introduction

Osteosarcoma (OS) is a malignant tumor of mesenchymal origin. The connective tissue of OS can directly induce tumor bone or osteoid tissue, mainly involving the metaphysis of the long bones [1]. In addition, as a primary sarcoma of the bone, OS is highly invasive, and easily metastasizes. In recent years, significant improvements have been made in the clinical diagnosis and treatment of OS, however, distant metastasis is often present at the time of initial diagnosis. Pulmonary metastasis is the most common, with a 5-year overall survival rate of less than 30% [2, 3]. At present, the occurrence, progression, and metastasis mechanisms of OS remain unclear. Therefore, an in-depth study of the mechanism of disease progression is of great significance for exploring new therapeutic targets and improving the outcome of OS.

Thioredoxin-interacting protein (TXNIP) is a member of the α-rhodopsin inhibitory protein family and is the only endogenous inhibitor in this family that can bind to thioredoxin [4]. TXNIP can regulate the levels of reactive oxygen species, promote inflammatory responses, and play an essential role in intracellular redox stress [5, 6]. In recent years, the non-redox pathway of TXNIP has attracted the attention of many researchers. TXNIP affects the growth state of cells through mitochondria-related energy metabolism pathways, and participates in cellular apoptosis, aging, differentiation, and proliferation [7]. In addition, TXNIP exerts biological functions, such as affecting tumor progression, regulating glucose and lipid metabolism, and mediating natural killer cell development, and is considered a key hub between metabolic reprogramming and tumor progression [8]. Previous studies have shown that TXNIP expression is downregulated in lung adenocarcinoma, hepatocellular carcinoma, gastric cancer, and other cancer cells, and inhibition of TXNIP expression promotes the malignant transformation of tumors [9, 10]. However, the role of TXNIP in OS remains to be explored,

and few studies have clarified its downstream targets and specific etiopathogenic mechanisms.

DNA damage-inducible transcript 4 (DDIT4) is also known to regulate development and DNA damage response 1 (REDD1). Originally discovered as a downstream target gene of hypoxia inducible HIF-1 [11], HIF-1 can induce its increased expression under conditions of DNA damage, hypoxia, nutrient consumption, and oxidative stress conditions [12], DDIT4 can participate in the regulation of cell survival by affecting DNA damage repair factor, HIF-1, mTOR, and other signaling pathways [13, 14]. In addition, DDIT4 is significantly correlated with tumor development, with significant differences in its expression levels having been described for a variety of malignancies [15]. The upregulated expression of DDIT4 can inhibit the formation of the downstream TSC1/TSC2 complex, negatively regulate the mechanistic target of rapamycin complex 1 (mTORC1), and inhibit the phosphorylation of its substrate protein S6, which exerts an anti-cancer function in tumor growth [16, 17]. However, this mechanism has not been confirmed in OS. Notably, previous studies have implicated the direct interaction between TXNIP and DDIT4 as a pathogenic mechanism of cardiovascular disease and oxidative stress [18, 19]. However, this relationship has not been explored in oncological settings.

This study demonstrated low levels of TXNIP expression in OS and its correlations with survival and prognosis. Furthermore, TXNIP was found to inhibit the phosphorylation of mTORC1 downstream target S6 through interaction with DDIT4 to restrain the proliferation, migration, and invasion of OS and promote apoptosis. Our results elucidate the interaction and regulatory mechanisms of TXNIP and DDIT4 in OS progression, and provide potential therapeutic targets for OS.

Material and methods

Patients and tissue samples

Tissue specimens were obtained from 90 patients with OS who underwent tumor resection and neoadjuvant chemotherapy at the Department of Orthopedics, Xiangya Hospital, Central South University. The paired collected OS tumor and adjacent tissues were derived from the pathological biopsy specimens before neoadjuvant chemotherapy, and stored at -80°C. The demographic data of the patients, including sex, age, tumor diameter, location, local recurrence, Enneking stage, metastasis, histology, and prognosis, were collected from the hospital's medical record management information system and used for statistical analysis. This study was approved by the Ethics Committee of Xiangya Hospital of Central South University, and informed consent was obtained from the patients and their legal guardians.

Cell lines and cell culture

The OS cell lines 143B, HOS, MG63, and U2OS, and the human osteoblastic cell line hFOB1.19 were obtained from the Xiangya cell repository. The cells were cultured in Dulbecco's modified Eagle's medium (Biological Industries, Israel) containing antibiotics and 10% fetal bovine serum (Gibco, USA) at 5% CO_2 and 37°C.

Immunohistochemistry (IHC)

Fresh OS and adjacent tissues were fixed with 4% paraformaldehyde and embedded in paraffin, and slices with a thickness of 6-8 μm were obtained. The slices were dewaxed with xylene for 20 min, rehydrated with an ethanol concentration gradient, and boiled in antigen repair solution for 20 min. The tissue was covered with a 3% hydrogen peroxide solution for 10 min to block endogenous peroxidase interference. Goat serum was applied for blocking for 1 h and then washed with a phosphate-buffered saline solution (PBST). Subsequently, primary antibodies (dilution ratio, 1:100) were added and incubated overnight in a refrigerator at 4°C. The solution was washed with PBST three times, and secondary antibodies (ABclonal, China) were added dropwise and incubated for 20 min. After washing, the slides were stained with DAB chromogenic reagent for 2 min and counterstained with hematoxylin for 2 min. Finally, after permeabilization with an ethanol concentration gradient, the slides were sealed with neutral gum and observed under a microscope. The antibodies used were TXNIP (Abcam, ab210826), BAX (CST, 14796S), Bcl-2 (CST, 15071S), and Ki-67 (Proteintech, 27309-1-AP).

Immunocytochemistry (ICC) and immunofluorescence (IF)

ICC and IF were performed as described in our previous studies [20]. For ICC, the cells were fixed with 4% paraformaldehyde. Dewaxing and antigen repair were also performed for IF. Incubation with primary antibodies (dilution ratio, 1:100, TXNIP, Abcam, UK) was performed overnight at 4°C, fluorescent secondary antibodies were used for binding for 1 h, and the cells were stained with DAPI for 5 min. After washing with PBS, images were captured using a Leica laser confocal microscope.

Reverse-transcriptase polymerase chain reaction (qRT-PCR)

A Trizol kit (CW Biotech, Beijing, China) was used to extract total RNA from tissues or cells, and cDNA was synthesized using a reverse transcription kit (Takara, Japan). Then, the cDNA was amplified using the qPCR system. Using GAPDH as a reference for data processing, the sequences of each target gene are shown in Table S1.

Western blotting (WB) and CO-IP

TPEB buffer (Invitrogen, Carlsbad, CA, USA) was used to extract tissue or cell proteins, and sample concentration was evaluated using the BCA method (Beyotime Biotechnology, Shanghai, China). We referred to our previous research on the specific operation process [21]. Briefly, protein samples were electrophoresed by SDS-PAGE and transferred to a polyvinylidene fluoride (PVDF) membrane. Sealing was completed with skim milk and the samples were incubated with the target antibodies. Luminescence was measured using an ECL kit. CO-IP with RIPA buffer (Thermo Fisher Scientific) was used to extract proteins from the input, IgG, and TXNIP/DDIT4 groups. Protein A/G magnetic beads (MedChemExpress, USA) were used to sort the protein complexes and obtain the protein supernatant for western blotting. The antibodies used were DDIT4 (Proteintech, 10638-1-AP), GAPDH (ABclonal, A19056), and β-actin (ABclonal, AC038). The remaining antibodies were consistent with our IHC results.

Lentiviral transduction and RNA interference

The overexpression lentivirus OE-TXNIP and the corresponding control lentivirus Con335 (Ubi-MCS-3FLAG-CBh-gcGFP-IRES-puromycin), the knockdown lentivirus sh1TXNIP, sh2TXNIP, and corresponding control Con313 (hU6-MCS-Ubiquitin-EGFP-IRES-puromycin), the transient plasmids for TXNIP (no GFP), the knockdown plasmid siDDIT4, and the corresponding control CTRL-si (hU6-MCS-CMV-Neomycin) were synthesized by Gikai GENE (Shanghai, China). The required concentration of the lentiviral solution was calculated to yield an MOI of 10, and cells were infected using 2 ug/mL puromycin for screening and 1 ug/ml puromycin to maintain the stable expression of cell lines. The plasmid was transfected using Lipofectamine 300 (Invitrogen, Carlsbad, CA, USA), and the intervention effect was observed after 48 h.

Cell proliferation and colony formation

As described in a previous study [22], the proliferation ability of cells was measured using the CCK-8 kit (Beyotime, China) and EdU kit (RiboBio, China). The cell suspension was prepared and seeded in a 96-well plate with a cell density of 3000 cells/well and 1.2×10^4 cells/well, respectively. The working solution from each kit was added at the corresponding time points. Cell proliferation was quantified using a multifunctional enzyme labeling instrument and fluorescence microscope. For colony formation experiments, cells were seeded in 6-well plates at a density of 1000 cells/well and cultured for 2 weeks.

Cell apoptosis assay

An Annexin V/PI kit (Vazyme, China) was used to detect apoptosis. 20×10^4 cells/well were planted in a 6-well plate. After 48 h, the plates were cleaned with PBS and the contents were added to a centrifuge tube. EDTA-free trypsin was added for digestion, and the cells were incubated with the binding buffer, annexin V, and PI for 1 h in the dark. Finally, the samples were analyzed using flow cytometry.

Transwell assay

A 24-well plate with a transwell chamber (Corning, NY, US) was used for the experiments. The cells were resuspended in serum-free cell culture medium and placed into the upper chamber (migration, 4×10^4 cells/well; invasion, 8×10^4 cells/well). The invasion experiment included Matrigel coating (dilution ratio, 1:8; BD), and the complete culture medi-

um was placed in the lower chamber. After 24 h of culture, the cells from the lower chamber were treated with 4% paraformaldehyde and crystal violet dye for 15 min, photographed, and counted under a microscope.

Scratch wound-healing assay

Transfected cells were seeded in 6-well plates (30×10^4 cells/well). When the cells reached approximately 80% confluence, a trace was scratched with a 10 μL tip head. After 24 h, images were captured using an inverted microscope and the transverse distance of the scratch was calculated.

Tumor xenograft models

Five-week-old female BALB/C nude mice were selected for tumor modelling, and HOS cell lines (4×10^6 cells/mouse) transfected with OE-TXNIP and Con335 were subcutaneously injected into the dorsal side of the nude mice. The tumor size was measured once per week. After 35 days, the nude mice were euthanized with 2% pentobarbital injection, and the tumors were collected and weighed. Subsequently, the tumor was embedded in paraffin and sectioned, and tissue proteins were extracted to detect the expression of relevant target molecules. This animal experiment was approved by the Experimental Animal Ethics Committee of Xiangya Hospital of Central South University.

Statistical methods

The Kaplan-Meier method and log-rank test were used to plot survival curves. Data collection and analysis were performed using SPSS 25.0, and quantitative statistical graphs were drawn using GraphPad Prism 8. All quantitative data were expressed as the mean ± standard deviation. The independent Student's t-test was used for comparisons between two groups, and one-way ANOVA was used to compare multiple groups. Qualitative data were expressed as frequencies, and statistical analysis was performed using the Chi-squared test or Fisher's exact test. Throughout this study, statistical significance was set at $P<0.05$.

Results

TXNIP downregulation in osteosarcoma is associated with a poor prognosis

HE staining demonstrated the classic cancer nest characteristics of OS tissues. *TXNIP* expression in OS tissues and adjacent tissues was detected by IHC staining, revealing that TXNIP was significantly underexpressed in OS (**Figure 1A**). Furthermore, the same results were obtained by IF staining analysis of OS and adjacent tissues; the red light representing TXNIP was significantly downregulated in OS tissues (**Figure 1B**). The proteins of OS and normal control (NC) tissues were extracted and detected by western blotting. These results further confirmed that TXNIP was significantly downregulated in OS tissues (**Figure 1C**). TXNIP mRNA expression in OS and NC tissues was analyzed using qRT-PCR. Compared to NC tissues, significantly lower TXNIP transcription levels were observed in OS tissues (**Figure 1D**). In addition, IHC was performed on the tumor tissues of 90 patients with OS, indicating that 53 patients showed relatively low TXNIP expression (**Figure 1E**). Survival prognostic analysis was performed using the Kaplan-Meier method and log-rank test, revealing that patients with low TXNIP expression had significantly lower overall survival and disease-free survival rates than those with high TXNIP expression (**Figure 1F**, **1G**). Statistical analysis of the clinicopathological features of these patients showed that the expression level of TXNIP correlated with tumor size, Enneking stage, and lung metastasis (**Table 1**).

Morphological expression of TXNIP in OS cell line and human normal osteoblast cell line hFOB1.19, as well as verification of transfection efficiency

An ICC experiment was performed to determine the specific expression and localization of TXNIP in OS cells compared to hFOB1.19. The OS cell lines, HOS, MG63, 143B, and U2OS, were expressed at low levels, and were mainly located in the cytoplasm (**Figure 2A**). In addition, the expression levels of TXNIP in the five cell lines were detected by qRT-PCR and western blotting, which confirmed that TXNIP was downregulated to various degrees in the four OS cell lines. Semi-quantitative analysis revealed that TXNIP expression was lowest in HOS cells and highest in MG63 cells (**Figure 2B**, **2C**). Therefore, the TXNIP-overexpressing lentivirus (OE-TXNIP) was transfected into the HOS cell line, and the TXNIP-knockdown lentivirus (sh1TXNIP, sh2TXNIP) was transfected into the MG63 cell line (**Figure 2D**). The post-transfection expression levels of TXNIP were detected by qRT-PCR and western blotting, indicating that TXNIP expression levels were signifi-

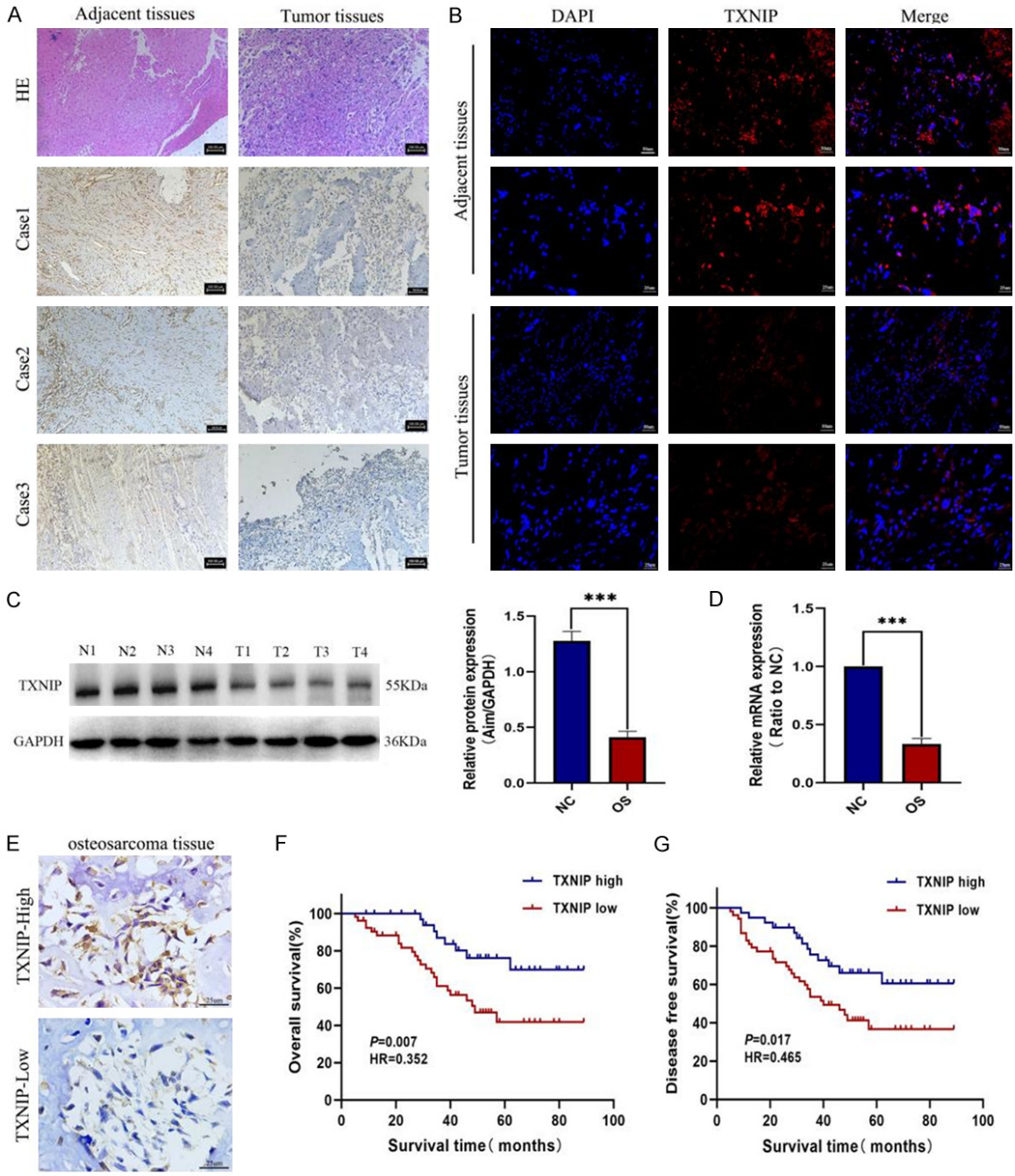

Figure 1. TXNIP is expressed in low amounts in OS tissue and is associated with survival prognosis. (A) HE staining showed the morphological characteristics of OS tissues and adjacent tissues, and the expression of TXNIP in OS tissues and adjacent tissues was detected by immunohistochemistry. Scale bar: 100 μm. (B) Tissue immunofluorescence showed the expression and localization of TXNIP in OS tissues and adjacent tissues. Scale bar: 25 μm. (C) WB analysis of the expression of TXNIP at the protein level in OS tissues and normal control tissues. (D) The mRNA expression of TXNIP in OS and normal control tissues was analyzed by qRT-PCR. (E) Representative images of high and low TXNIP expression in OS tissues. Scale bar: 25 μm. (F, G) Overall survival (F) and disease-free survival rate (G) in patients with OS. Data from at least 3 independent replicate experiments. Results are expressed as mean ± SD. ***P<0.001, vs. Control, by Student's t-test.

cantly upregulated and silenced in the transfected HOS and MG63 cell lines, which reached the standards of subsequent experiments (**Figure 2E-G**).

Table 1. Correlation of TXNIP expression with clinicopathological features of OS patients

Clinicopathological parameter	TXNIP protein expression		*P* value
	Low (n = 53)	High (n = 37)	
Age			0.924
<21	44	31	
≥21	9	6	
Sex			0.813
Female	17	11	
Male	36	26	
Tumour size (cm)			0.045
<8	23	24	
≥8	30	13	
Local recurrence			0.553
Yes	6	2	
No	47	35	
Enneking's stage			0.011
IIA	8	5	
IIB	25	28	
III	20	4	
Anatomic location			0.685
Femur	27	15	
Tibia	14	10	
Humerus	8	9	
Others	4	3	
Lung metastasis			0.004
Yes	24	6	
No	29	31	
Histology			0.909
Conventional osteosarcoma	41	29	
Others	12	8	

Differences between groups were done by the Chi-square test.

TXNIP can inhibit the proliferation, migration and invasion of OS cells and promote their apoptosis in vitro

CCK-8 and EdU assays were performed to investigate the specific function of TXNIP in OS progression. The results indicated that the proliferation of the HOS cell line transfected with OE-TXNIP lentivirus was significantly inhibited. However, increased proliferation of MG63 cells transfected with TXNIP shRNA lentivirus was observed (**Figure 2H**, **2I**). Consistently, compared with the empty vector group, the number of clones formed was significantly lower in HOS cells with TXNIP overexpression and significantly higher in MG63 cells with TXNIP knockdown (**Figure 3A**, **3B**). Furthermore, the apoptosis assay indicated that TXNIP overexpression promoted the apoptosis of HOS cells, upregulated the apoptosis marker protein Bax, and inhibited the expression of Bcl-2 (**Figure 3C**, **3E**), whereas silencing TXNIP in MG63 cells showed the opposite trend and inhibited apoptosis. Compared to the Con313 group, Bax expression was downregulated and Bcl-2 expression was upregulated (**Figure 3D**, **3F**). Moreover, transwell and scratch wound-healing assays confirmed that migration and invasion were significantly inhibited in HOS cells with upregulated TXNIP (**Figure 3G**, **3I**, **3K**). However, migration and invasion abilities were enhanced in the two TXNIP-silenced MG63 cell groups (**Figure 3H**, **3J**, **3L**). These results indicated that TXNIP inhibits the growth and metastasis of OS cells and plays an inhibitory role in OS progression.

TXNIP suppresses OS cell growth and proliferation in xenograft mice

The tumor-inhibitory effects of TXNIP were further investigated in vivo. The same number of HOS cells stably transfected with Con-335 and OE-TXNIP was transplanted subcutaneously into nude mice, and tumor growth was monitored and measured every 7 days. On day 28 after inoculation, the size of the subcutaneous tumors was observed using in vivo imaging. A significant difference in tumor size was observed between the Con335 and OE-TXNIP groups (**Figure 4A**). On day 35, tumors were collected and weighed. Tumor size and weight in the control group were significantly larger than those in the OE-TXNIP group (**Figure 4B**). Extraction of tissue proteins from both groups followed by western blotting results showed that the expression of TXNIP and Bax was significantly upregulated, and Bcl-2 was significantly downregulated, in the OE-TXNIP group (**Figure 4C**). Subsequently, the tumor tissue was stained with HE and IHC was performed, demonstrating that the cancer nests formed in the OE-TXNIP group were relatively

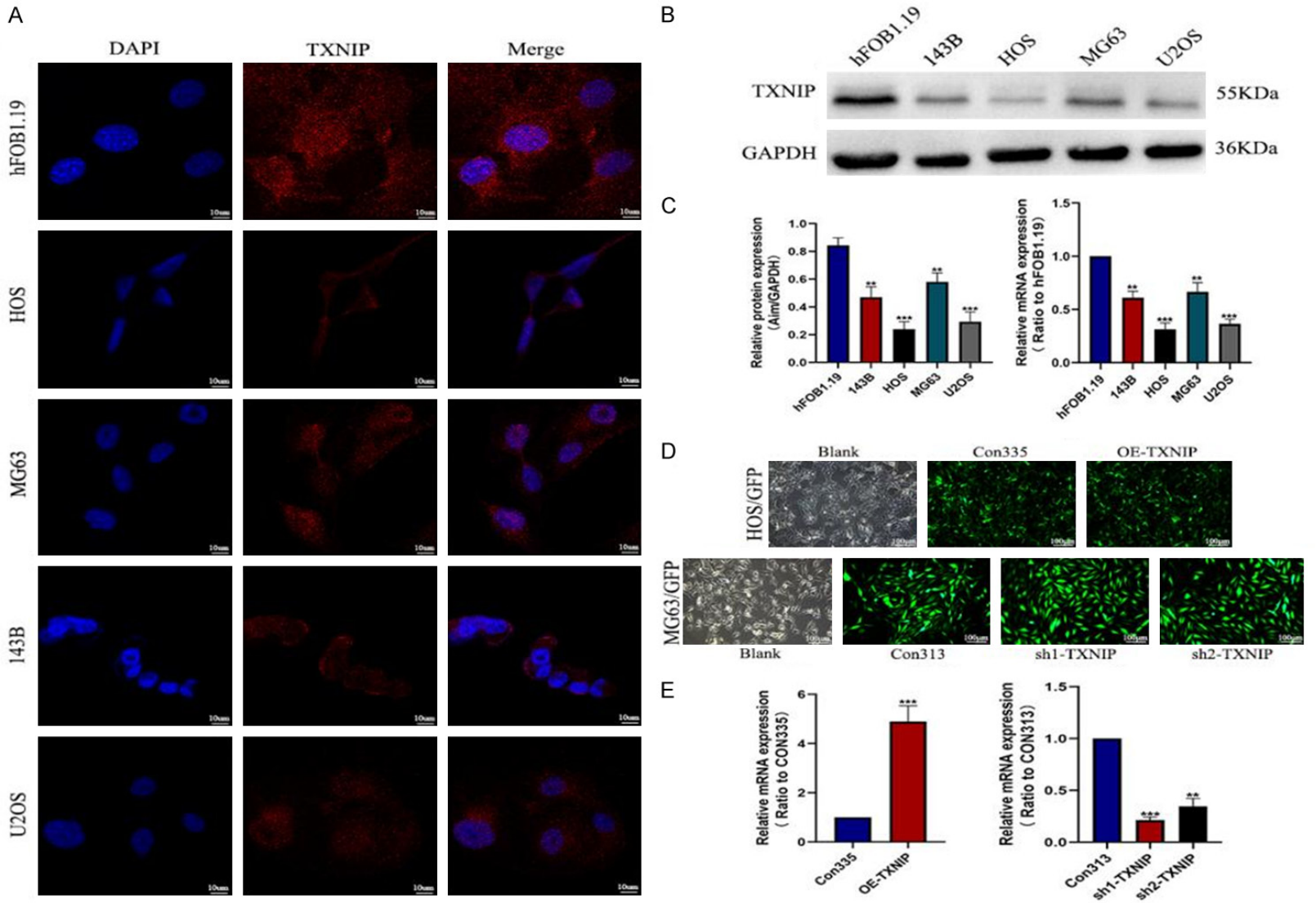
A
DAPI
TXNIP
Merge
hFOB1.19
HOS
MG63
143B
U2OS
B
hFOB1.19
143B
HOS
MG63
U2OS
TXNIP
55KDa
GAPDH
36KDa
C
Relative protein expression (Aim/GAPDH)
Relative mRNA expression (Ratio to hFOB1.19)
D
Blank
Con335
OE-TXNIP
HOS/GFP
MG63/GFP
Blank
Con313
sh1-TXNIP
sh2-TXNIP
E
Relative mRNA expression (Ratio to CON335)
Con335
OE-TXNIP
Relative mRNA expression (Ratio to CON313)
Con313
sh1-TXNIP
sh2-TXNIP

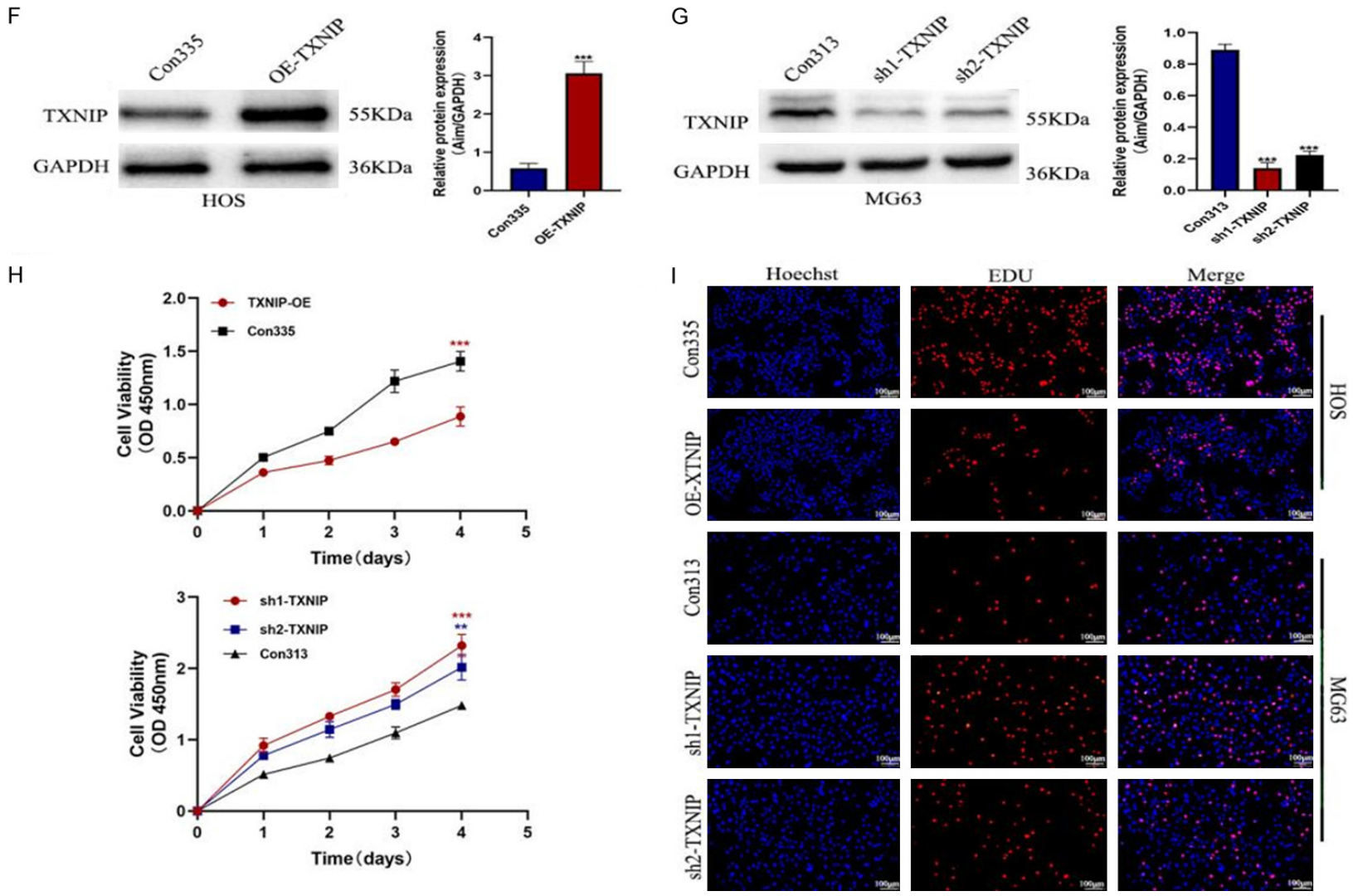

Figure 2. The expression and localization of TXNIP in OS cells, and can inhibit the proliferation of OS cells. (A) From the observation of cell immunofluorescence, the expression of TXNIP is mainly located in the cytoplasm, the nucleus is stained with DAPI, and the TXNIP protein is marked in red. Scale bar: 10 μm. (B, C) The proteins and mRNAs of four OS cell lines and human normal osteoblast cell line hFOB1.19 were extracted and analyzed by WB (B) and qRT-PCR (C). (D) Lentiviruses with GFP that up-regulated or knocked down TXNIP were transfected into HOS cells and MG63 cells, respectively. Scale bar: 100 μm. (E-G) Using qRT-PCR (E) and WB to evaluate the overexpression efficiency of TXNIP in HOS cells (F) and the silencing efficiency of TXNIP in MG63 cells (G). (H) CCK-8 was used to detect the growth of OS cells after TXNIP overexpression and knockdown. (I) EdU was used to detect the proliferation of OS cells after TXNIP overexpression or knockdown. Scale bar: 100 μm. Data from 3 independent replicate experiments. Results are expressed as mean ± SD. **P<0.01, ***P<0.001, vs. Control, by Student's t-test.

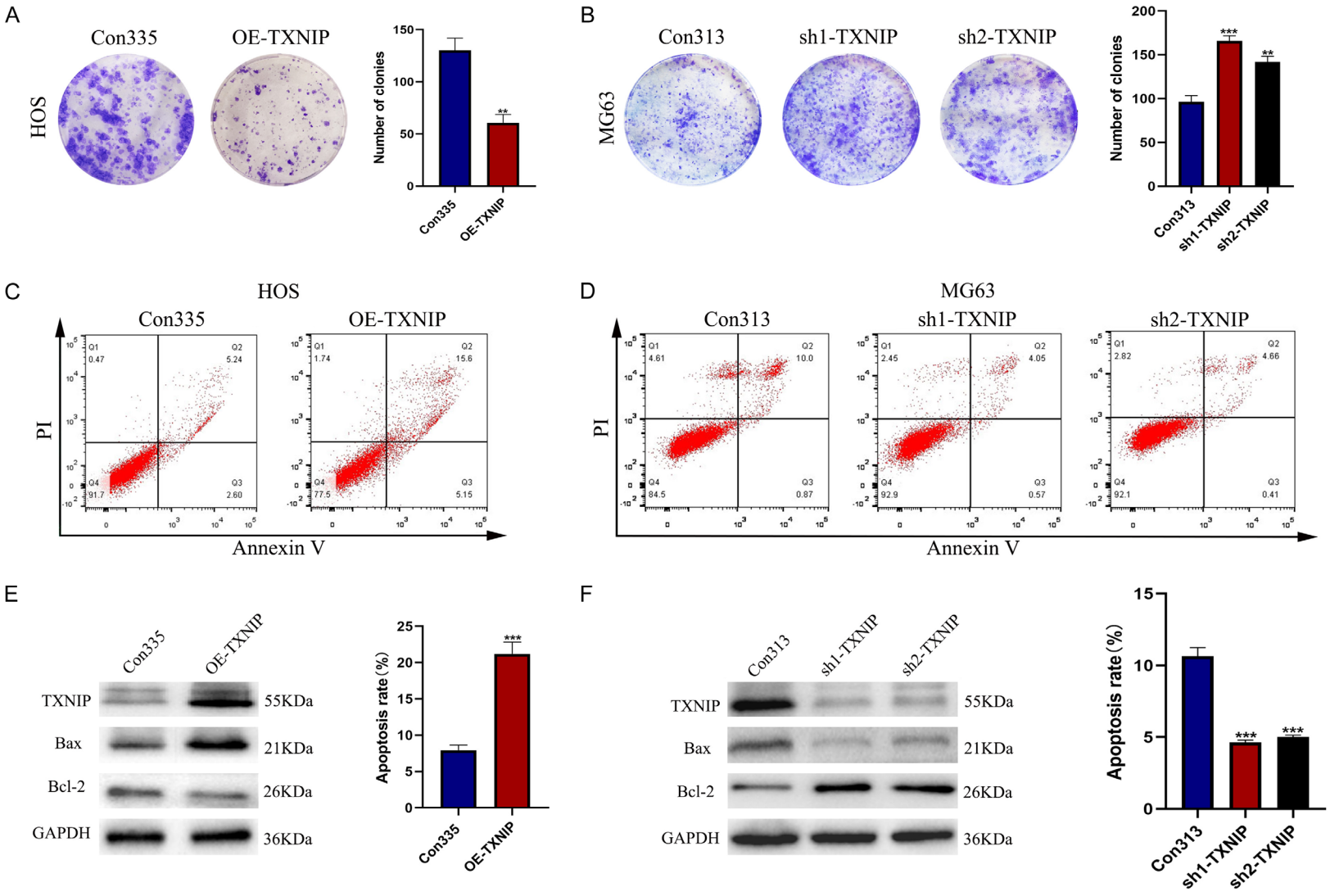
A
Con335
OE-TXNIP
HOS
Number of clonies
150
100
50
0
**
Con335
OE-TXNIP
B
Con313
sh1-TXNIP
sh2-TXNIP
MG63
Number of clonies
200
150
100
50
0
***
**
Con313
sh1-TXNIP
sh2-TXNIP
C
HOS
Con335
OE-TXNIP
PI
Annexin V
Q1 0.47
Q2 5.24
Q4 91.7
Q3 2.60
Q1 1.74
Q2 15.6
Q4 77.5
Q3 5.15
D
MG63
Con313
sh1-TXNIP
sh2-TXNIP
PI
Annexin V
Q1 4.61
Q2 10.0
Q4 84.5
Q3 0.87
Q1 2.45
Q2 4.05
Q4 92.9
Q3 0.57
Q1 2.82
Q2 4.66
Q4 92.1
Q3 0.41
E
Con335
OE-TXNIP
TXNIP
Bax
Bcl-2
GAPDH
55KDa
21KDa
26KDa
36KDa
Apoptosis rate (%)
25
20
15
10
5
0
***
Con335
OE-TXNIP
F
Con313
sh1-TXNIP
sh2-TXNIP
TXNIP
Bax
Bcl-2
GAPDH
55KDa
21KDa
26KDa
36KDa
Apoptosis rate (%)
15
10
5
0
***
***
Con313
sh1-TXNIP
sh2-TXNIP

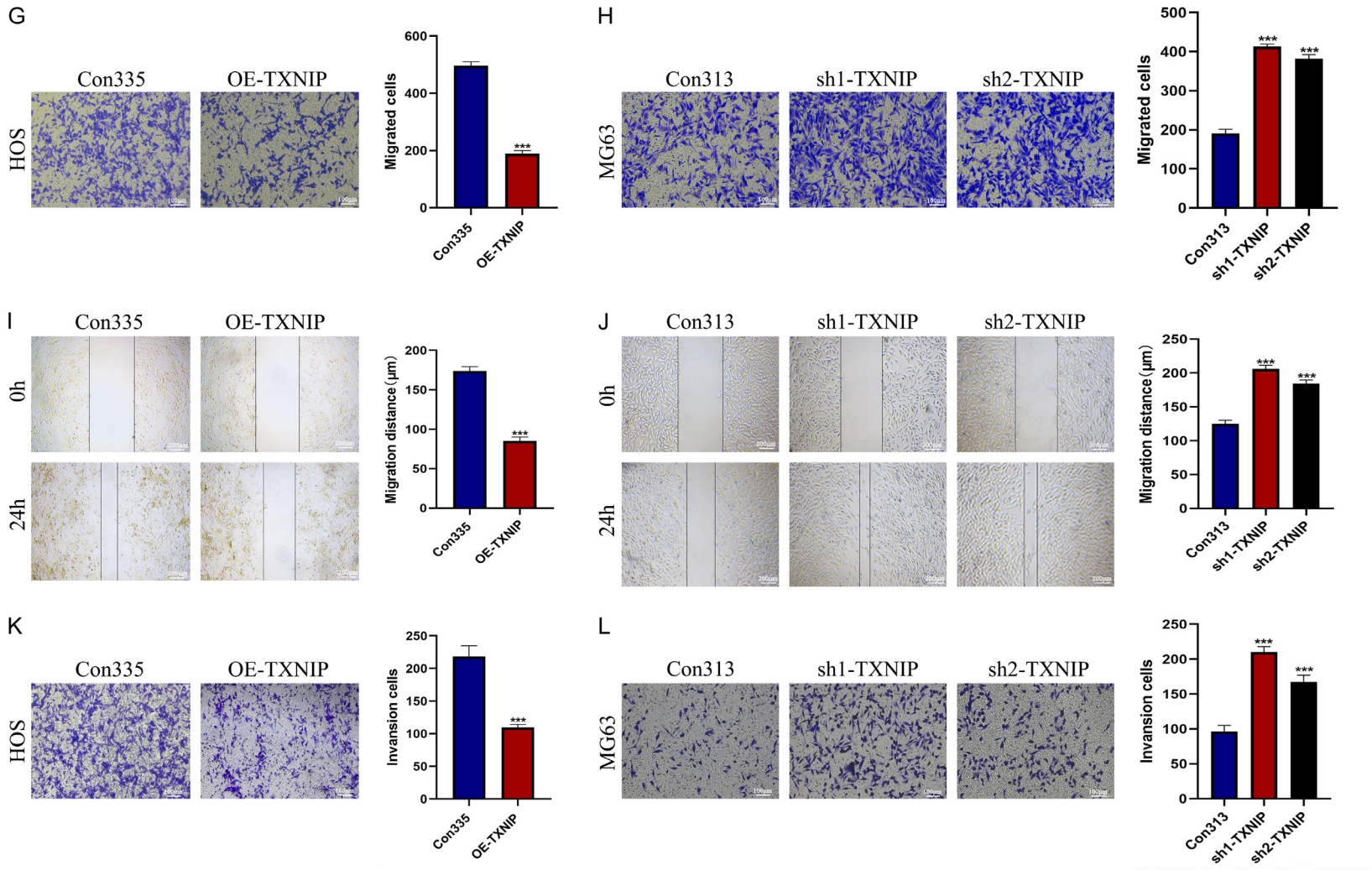

Figure 3. TXNIP can inhibit the colony formation, migration and invasion of OS cells and promote their apoptosis. (A, B) In HOS (A) and MG63 cells (B), TXNIP overexpression or knockdown affected the formation of cell colonies. (C, D) Altering the expression of TXNIP affects the apoptosis of HOS (C) and MG63 cells (D). (E) WB was used to verify the effect of overexpression of TXNIP on apoptosis-related proteins Bax and Bcl-2 in HOS cells. (F) WB was used to confirm the effect of knockdown of TXNIP on apoptosis-related proteins Bax and Bcl-2 in MG63 cells. (G, I) Transwell experiments (G) and scratch experiments (I) demonstrating the effect of TXNIP overexpression on the migratory ability of HOS cells. Scale bar: 100 μm (G) or 200 μm (I). (H, J) Transwell experiments (H) and scratch experiments (J) displaying the effect of TXNIP knockdown on the migratory ability of MG63 cells. Scale bar: 100 μm (H) or 200 μm (J). (K, L) Effect of TXNIP up-regulation or down-regulation on the invasion ability of HOS (K) and MG63 (L) cells. Scale bar: 100 μm. Data from 3 independent replicate experiments. Results are expressed as mean ± SD. **P<0.01, ***P<0.001, vs. Control, by Student's t-test.

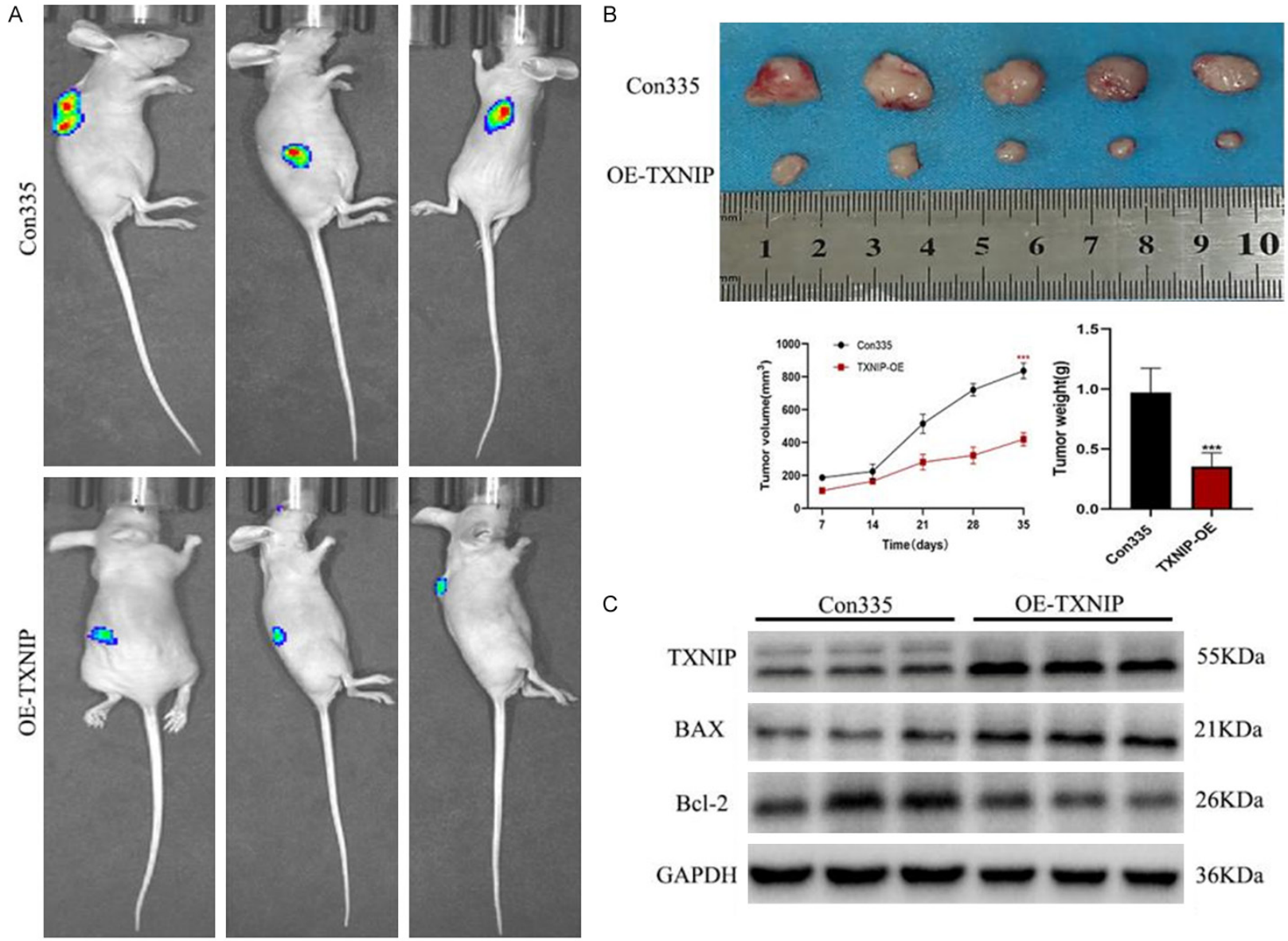
A
Con335
OE-TXNIP
B
Con335
OE-TXNIP
1 2 3 4 5 6 7 8 9 10
Con335
TXNIP-OE
Tumor volume(mm3)
Time (days)
Tumor weight(g)
Con335
TXNIP-OE
C
Con335
OE-TXNIP
TXNIP
BAX
Bcl-2
GAPDH
55KDa
21KDa
26KDa
36KDa

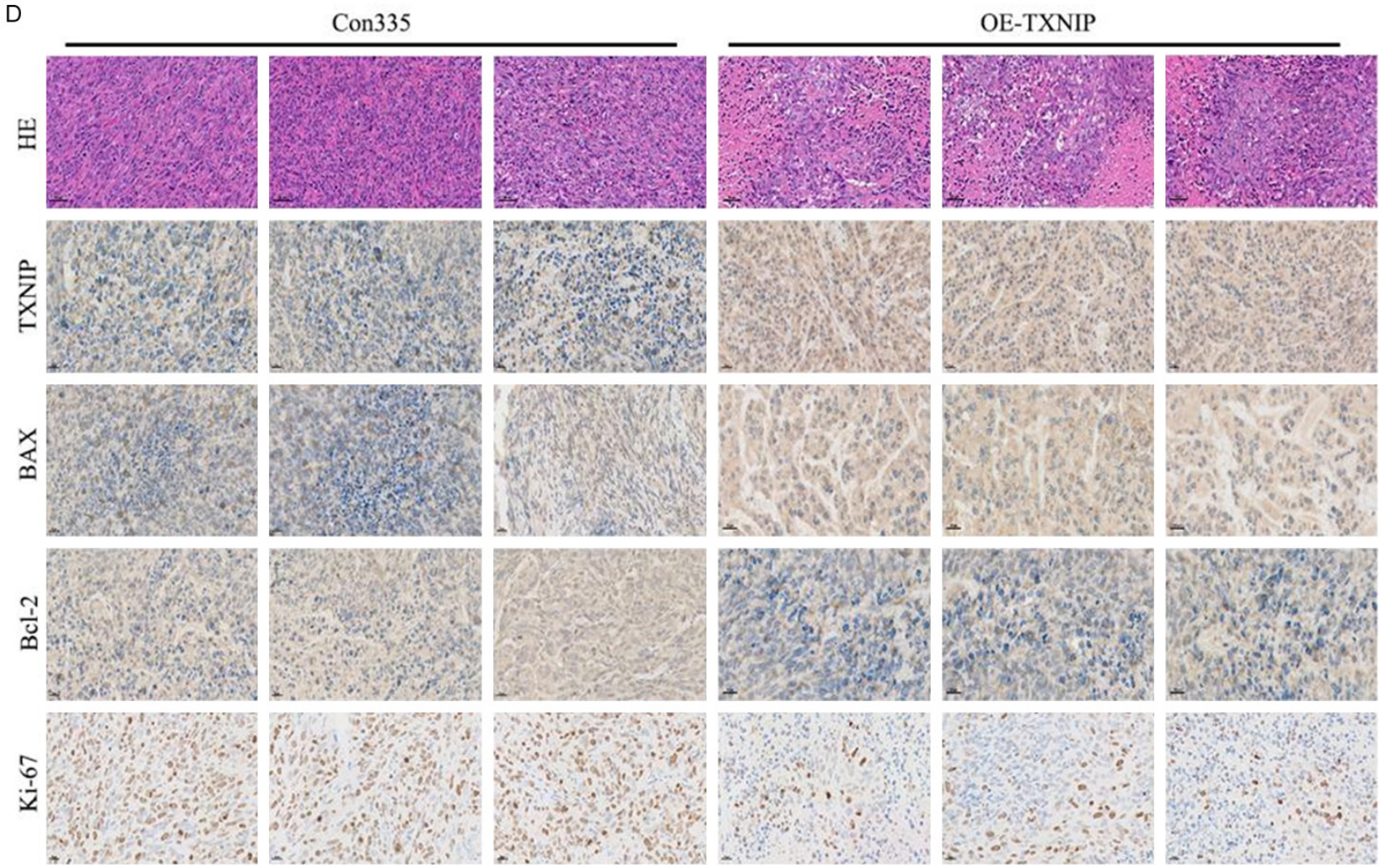

Figure 4. Overexpression of TXNIP can inhibit the growth of xenograft tumors. A. Live imaging experiments showed the inhibitory effect of TXNIP overexpression on subcutaneous xenograft tumors. B. Differences in size, weight and growth curve of subcutaneous tumors in Con 335 and OE-TXNIP groups. C. WB detected the differences in TXNIP, Bax and Bcl-2 expression in nude mouse tumors in the Con 335 and OE-TXNIP groups. D. Differential expression of TXNIP, BAX, Bcl-2, and Ki67 in subcutaneous tumors was determined by immunohistochemistry on the Con 335 and OE-TXNIP group. Scale bar: 20 μm. Data from at least 3 independent replicate experiments. Results are expressed as mean ± SD. ***P<0.001, vs. Control, by Student's t-test.

atypical. IHC staining of TXNIP and Bax showed a noticeable dark brown color with a high expression level, while the expression of Bcl-2 and Ki-67 was relatively low (**Figure 4D**). These results suggest that TXNIP overexpression inhibits OS development in vivo.

TXNIP directly binds to DDIT4 and positively regulates its expression, thus inhibiting phosphorylation of mTORC1 downstream substrate S6

To further clarify the downstream pathways of TXNIP that are involved in its tumor suppressor effect, the protein interaction network of TXNIP was analyzed using the STRING database (**Figure 5A**). Although the interaction between DDIT4 and TXNIP has been confirmed in cardiovascular disease and oxidative stress-related research [18, 19], this relationship remains unexplored in oncology. Therefore, DDIT4 was included as the candidate gene. We First, CO-IP experiments were performed to confirm that TXNIP can bind to DDIT4 in OS cells (**Figure 5B**). Second, a TXNIP-overexpressing plasmid was transiently transfected into HOS cells and a TXNIP-knockout plasmid was transiently transfected into MG63 cells. Furthermore, immunofluorescence revealed that TXNIP and DDIT4 co-existed in the cytoplasm. Obvious yellow fluorescence was observed in the cells after merging, which further supported the direct physical connection between TXNIP and DDIT4 (**Figure 5C**, **5D**). Moreover, western blotting and qRT-PCR results indicated that, compared with the control group, the expression of DDIT4 in the OE-TXNIP group was significantly upregulated, and the phosphorylation of the downstream substrate S6 of mTORC1 was inhibited (**Figure 5E**, **5G**). Correspondingly, DDIT4 expression was inhibited in both the sh1-TXNIP and sh2-TXNIP groups, while S6 phosphorylation was activated (**Figure 5F**, **5G**). Based on these data, the DDIT4 knockdown plasmid siDDIT4 and its control empty vector CTRL-si were transfected into the Con335 and OE-TXNIP groups, respectively. Semi-quantitative analysis revealed that in TXNIP overexpression, downregulation of DDIT4 significantly reversed the phosphorylation of S6 (**Figure 5H**). Therefore, it can be considered that DDIT4 mediates the inhibitory effect of TXNIP on mTORC1.

DDIT4 is a key downstream target of TXNIP for its tumor suppressor effect

To determine whether DDIT4 is a functional downstream gene of TXNIP, the phenotypes of the four groups of HOS cells were examined. The CCK-8 and EdU results showed that knockdown of DDIT4 in Con335 HOS cells slightly increased their proliferation ability, but the difference was not statistically significant. After transduction of siDDIT4 into OE-TXNIP HOS cells, it was found that knockdown of DDIT4 significantly reversed the inhibition of HOS cell proliferation by TXNIP (**Figure 6A-C**). A transwell assay was performed to evaluate the migration and invasion of HOS cells in each group. Following TXNIP overexpression, silencing the expression of DDIT4 reversed the migration and invasion abilities of the cells. However, silencing of DDIT4 had little effect on the migration ability of HOS cells (**Figure 6D**). Notably, apoptosis flow cytometry results also indicated that siDDIT4 attenuated most of the pro-apoptotic effects of TXNIP in HOS cells (**Figure 6E**). Collectively, these findings suggest that TXNIP inhibits OS progression via DDIT4-mediated mTORC1 suppression (**Figure 6F**).

Discussion

OS is a complex process involving various molecular changes. Genetic changes and abnormal regulation of various cellular signaling pathways are major events that result in high invasiveness, metastasis rate, and mortality in OS [23, 24]. TXNIP is a thioredoxin-binding protein that exerts a variety of biological functions in the human body, including endocrine metabolism, transcriptional regulation of intracellular genes, regulation of a variety of stress reactions, and taking part in the development of natural killer cells. TXNIP can affect the response pathway of reactive oxygen species in mitochondria to regulate cell proliferation and apoptosis [5]. Recently, many studies have found that abnormal expression of TXNIP plays an essential role in the progression of various tumors and is correlated with clinical prognosis [8, 25]. However, no in-depth study has been performed on OS. In this study, we first confirmed low mRNA and protein expression of TXNIP in human OS tissue samples and OS cell lines. Low TXNIP expression was highly correlated with tumor stage, distant metasta-

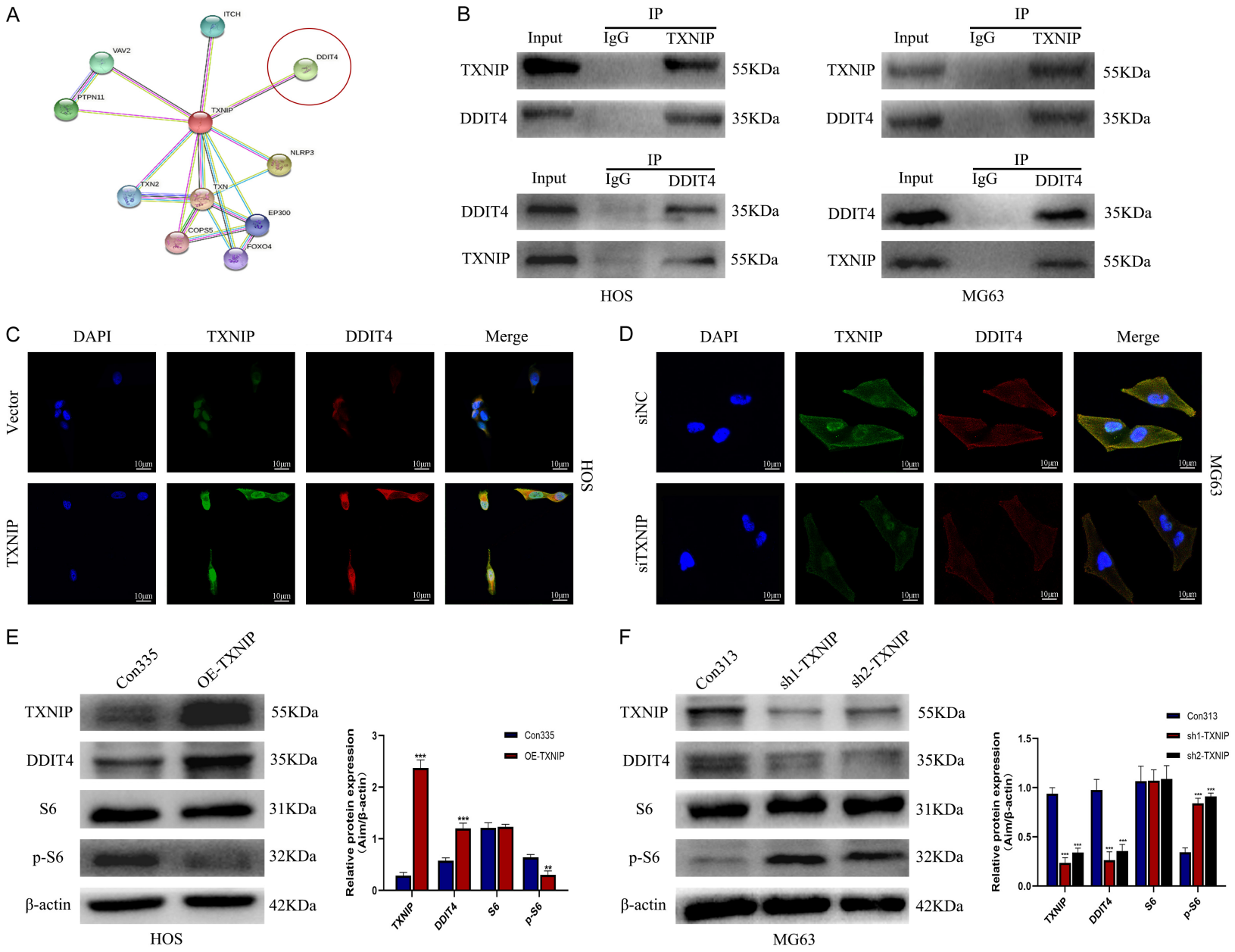
A
ITCH
VAV2
DDIT4
PTPN11
TXNIP
NLRP3
TXN2
TXN
EP300
COPS5
FOXO4
B
IP
Input
IgG
TXNIP
DDIT4
55KDa
35KDa
HOS
MG63
C
DAPI
TXNIP
DDIT4
Merge
Vector
TXNIP
10μm
HOS
D
siNC
siTXNIP
MG63
E
Con335
OE-TXNIP
S6
p-S6
β-actin
31KDa
32KDa
42KDa
Relative protein expression (Aim/β-actin)
F
Con313
sh1-TXNIP
sh2-TXNIP

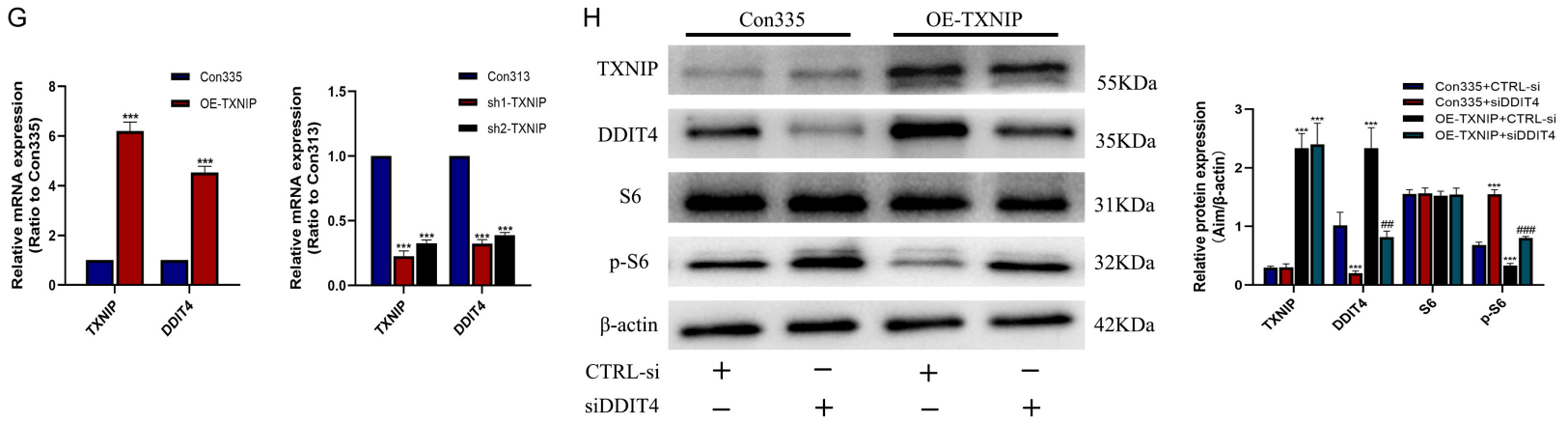

Figure 5. DDIT4 is the downstream target of TXNIP. (A) The protein interaction prediction network of TXNIP was obtained from the STRING database. (B) The protein lysates of HOS and MG63 cells were subjected to CO-IP with anti-TXNIP, anti-DDIT4, or control IgG antibodies, respectively. (C, D) The co-localization of TXNIP and DDIT4 in HOS (C) and MG63 cells (D) was analyzed by cellular immunofluorescence confocal. Scale bar: 10 μm. (E, F) The expression of TXNIP, DDIT4, S6 and p-S6 was detected by WB in OE-TXNIP HOS cells (E), sh-TXNIP MG63 cells (F) and their control groups. (G) The transcription of TXNIP and DDIT4 in each intervention group was detected by qRT-PCR. (H) WB analysis showed the effects of transduction of OE-TXNIP lentivirus and/or si-DDIT4 plasmid on the expression of TXNIP, DDIT4, S6 and p-S6 in HOS cells. Data from 3 independent replicate experiments. Results are expressed as mean ± SD. **P<0.01, ***P<0.001, vs. Control. ##P<0.01, ###P<0.001, vs. OE-TXNIP+CTRL-si, by one-way ANOVA.

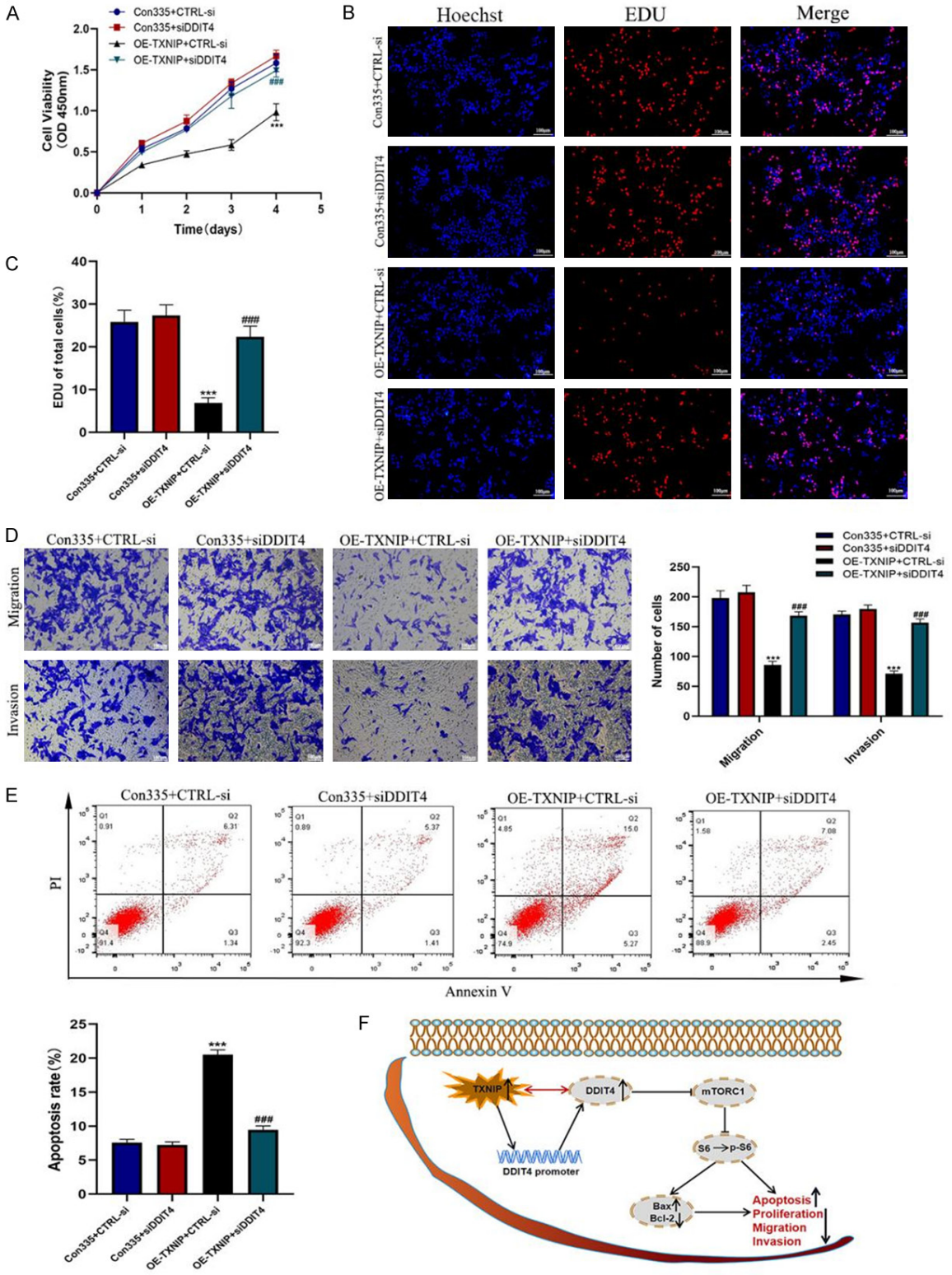

Figure 6. TXNIP exerts a tumor suppressor effect on OS cells by targeting DDIT4. (A) CCK-8 detects the effect of transduction of OE-TXNIP lentivirus and/or si-DDIT4 plasmid on the growth of HOS cells. (B, C) Representative images (B) and quantitative analysis (C) of EdU results in HOS cells transduced with OE-TXNIP lentivirus and/or si-DDIT4 plasmid. Scale bar: 100 μm. (D) Transwell assay showed the effect of transduction of OE-TXNIP lentivirus and/or si-DDIT4 plasmid on the migration and invasion of HOS cells. Scale bar: 100 μm. (E) Flow cytometry results reveal the effect of transduction of OE-TXNIP lentivirus and/or si-DDIT4 plasmid on the apoptotic effect of HOS cells. (F) Sche-

matic diagram of TXNIP targeting DDIT4 to exert its tumor suppressor effect. Data from 3 independent replicate experiments. Results are expressed as mean ± SD. ***P<0.001, vs. Control. ###P<0.001, vs. OE-TXNIP+CTRL-si, by one-way ANOVA.

sis, tumor size, and poor prognosis in patients with OS. Our results indicated that TXNIP may be a prognostic marker for OS.

Next, we explored the specific function of TXNIP in OS. Previous studies have reported low TXNIP expression in various tumor tissues compared to the corresponding adjacent tissues. TXNIP can inhibit the development of solid malignant tumors, such as breast cancer, renal cell carcinoma, lung cancer, and gastric cancer [26, 27] through the involvement of multiple signaling pathways. TXNIP is also considered to be involved in tumor energy metabolism, cell senescence and immune microenvironment [28, 29]. Cell phenotype experiments demonstrated that TXNIP overexpression inhibited the proliferation, migration, and invasion of OS cells, and promoted their apoptosis. In contrast, TXNIP knockdown promoted OS cell proliferation, migration, and invasion and inhibited apoptosis. Furthermore, a xenograft model of OS was established in nude mice. TXNIP significantly inhibits tumor growth. Therefore, the inhibitory role of TXNIP in the progression of OS was confirmed, which is consistent with relevant studies conducted in other cancers.

However, studies on the mechanism underlying TXNIP inhibition of cancer progression are scarce, and the downstream pathways remain unknown. In the TXNIP protein network, DDIT4 plays a similar role in many non-tumor diseases and mechanisms. For example, DDIT4 can positively regulate the production of intracellular reactive oxygen species, and participate in DNA damage repair, lipid metabolism, the inflammatory response, and autophagy [30, 31]. Under normal circumstances, DDIT4 is generally expressed in low amounts in most adult tissues, and its expression is regulated by many factors [32]. Previous studies have shown that DDIT4 mainly exists in the cytoplasm and has obvious co-localization with mitochondria, which may provide the structural basis for the functional relationship between TXNIP and DDIT4 [33]. Moreover, recent studies on DDIT4 have investigated its potential as a new tumor-related target. Significant differences among the expression levels in malignant tumors, such as lung, bladder, and ovarian cancers, were initially found. Furthermore, DDIT4 is involved in the prognostic evaluation of breast cancer and lymphoma [34, 35]. Moreover, DDIT4 can also affect antitumor drug tolerance by regulating autophagy and can interfere with temozolomide, radiotherapy, and hypoxia-induced tumor cell death [11]. However, the specific functional mechanisms are still unclear. Interestingly, some studies have confirmed the existence of the TXNIP/DDIT4 axis in apoptosis, hypoxic stress, mitochondrial metabolism, cell movement, and injury [18, 19]. Under conditions of aerobic exercise, TXNIP was found to affect DDIT4 expression by regulating the levels of reactive oxygen species in mitochondria [36], however, further studies have confirmed that TXNIP can directly bind to DDIT4 to regulate its synthesis, and then participate in redox reactions, ischemia and reperfusion injury, autophagy activation, and other mechanisms [18, 37]. In these studies, relevant experiments, such as bioletter data analysis and CO-IP provide a strong argument, and the connection between TXNIP and DDIT4 in OS should be further explored. First, we confirmed the direct physical binding relationship between TXNIP and DDIT4 in OS cells through CO-IP and ICC experiments. Western blotting and qRT-PCR experiments revealed that the expression of DDIT4 was positively correlated with TXNIP and inhibited the phosphorylation of the mTORC1 downstream substrate S6. Multiple studies have shown that inactivation of mTORC1 can hinder the phosphorylation of the downstream factor S6, thereby suppressing tumor growth and basal metabolism [38, 39]. As an endogenous inhibitor of mTORC1, DDIT4 is likely to mediate the tumor suppressor pathway of TXNIP through this classical target. Therefore, it is reasonable to assume that there is a signal regulation axis of TXNIP/DDIT4/mTORC1/p-S6 in OS.

We then knocked down DDIT4 while overexpressing TXNIP, which restored the phosphorylation of S6. After transduction of siDDIT4 into OE-TXNIP HOS cells, downregulation of DDIT4 significantly reversed the inhibitory effect of TXNIP on the proliferation, migration, and inva-

sion of HOS cells. Moreover, it significantly attenuated the pro-apoptotic effects of TXNIP on HOS cells. However, the downregulation of DDIT4 itself did not affect the functional phenotype of HOS cells. Therefore, the anti-tumor effect of TXNIP is mainly mediated by the DDIT4/mTORC1/p-S6 pathway. Other signaling molecules may also participate in the TXNIP-DDIT4 signaling axis. In addition, some studies suggest that DDIT4 interacts with TXNIP to participate in the fate and outcome of cells [40, 41], which requires further research. Further analysis of the molecular mechanism of the TXNIP-DDIT4 signaling axis will provide a theoretical and experimental basis for the combined application of antitumor drugs targeting TXNIP and DDIT4 in clinical practice.

In summary, the expression, biological function, and downstream regulatory mechanism of TXNIP in OS were verified for the first time. This study found that TXNIP was underexpressed in OS tissues and cells, and was associated with poor overall and disease-free survival in patients with OS. In addition, TXNIP can control the proliferation, migration, and invasion of OS cells and promote their apoptosis by upregulating DDIT4 and inhibiting the phosphorylation of mTORC1 downstream substrate S6. Thus, TXNIP/DDIT4/mTORC1 suppression was identified as the mechanism of inhibiting malignant biological behavior in OS.

Acknowledgements

We are grateful for financial supports from the construction of innovative provinces in Hunan Province (No. 2020RC3058), Joint funds of hospitals and enterprises (No. DK-KYHT20-22041901 and No. HFKC-KY-20220601).

Disclosure of conflict of interest

None.

Abbreviations

OS, osteosarcoma; TXNIP, thioredoxin-interacting protein; DDIT4, DNA damage-inducible transcript 4; REDD1, regulated in development and DNA damage response 1; mTORC1, mechanistic target of rapamycin complex 1; IHC, immunohistochemistry; ICC, Immunocytochemistry; IF, Immunofluorescence; WB, Western blotting; NC, normal control.

Address correspondence to: Dr. Wei Luo, Department of Orthopaedics, Xiangya Hospital, Central South University, Changsha 410008, Hunan, P. R. China. Tel: +86-15116329088; E-mail: luowei09-28@126.com

References

[1] Yang Z, Guo Q, Cai Y, Zhu X, Zhu C, Li Y and Li B. Poly(ethylene glycol)-sheddable reduction-sensitive polyurethane micelles for triggered intracellular drug delivery for osteosarcoma treatment. J Orthop Translat 2019; 21: 57-65.

[2] Verschoor AJ, Speetjens FM, Dijkstra PDS, Fiocco M, van de Sande MAJ, Bovée JVMG and Gelderblom H. Single-center experience with ifosfamide monotherapy as second-line treatment of recurrent/metastatic osteosarcoma. Oncologist 2020; 25: e716-e721.

[3] Bian ZJ, Shan HJ, Zhu YR, Shi C, Chen MB, Huang YM, Wang XD, Zhou XZ and Cao C. Identification of Galphai3 as a promising target for oste-osarcoma treatment. Int J Biol Sci 2022; 18: 1508-1520.

[4] Iqbal MA, Chattopadhyay S, Siddiqui FA, Ur Rehman A, Siddiqui S, Prakasam G, Khan A, Sultana S and Bamezai RN. Silibinin induces metabolic crisis in triple-negative breast cancer cells by modulating EGFR-MYC-TXNIP axis: potential therapeutic implications. FEBS J 2021; 288: 471-485.

[5] Zhou R, Tardivel A, Thorens B, Choi I and Tschopp J. Thioredoxin-interacting protein links oxidative stress to inflammasome activation. Nat Immunol 2010; 11: 136-140.

[6] Tsubaki H, Tooyama I and Walker DG. Thioredoxin-interacting protein (TXNIP) with focus on brain and neurodegenerative diseases. Int J Mol Sci 2020; 21: 9357.

[7] Ismael S, Nasoohi S, Li L, Aslam KS, Khan MM, El-Remessy AB, McDonald MP, Liao FF and Ishrat T. Thioredoxin interacting protein regulates age-associated neuroinflammation. Neurobiol Dis 2021; 156: 105399.

[8] Chen Y, Ning J, Cao W, Wang S, Du T, Jiang J, Feng X and Zhang B. Research progress of TXNIP as a tumor suppressor gene participating in the metabolic reprogramming and oxidative stress of cancer cells in various cancers. Front Oncol 2020; 10: 568574.

[9] Liang Y, Wang H, Chen B, Mao Q, Xia W, Zhang T, Song X, Zhang Z, Xu L, Dong G and Jiang F. circDCUN1D4 suppresses tumor metastasis and glycolysis in lung adenocarcinoma by stabilizing TXNIP expression. Mol Ther Nucleic Acids 2021; 23: 355-368.

[10] Zhang Y, Yan Q, Gong L, Xu H, Liu B, Fang X, Yu D, Li L, Wei T, Wang Y, Wong CN, Lyu Z, Tang Y, Sham PC and Guan XY. C-terminal truncated

HBx initiates hepatocarcinogenesis by down-regulating TXNIP and reprogramming glucose metabolism. Oncogene 2021; 40: 1147-1161.
[11] Foltyn M, Luger AL, Lorenz NI, Sauer B, Mittelbronn M, Harter PN, Steinbach JP and Ronellenfitsch MW. The physiological mTOR complex 1 inhibitor DDIT4 mediates therapy resistance in glioblastoma. Br J Cancer 2019; 120: 481-487.
[12] Savukaitytė A, Gudoitytė G, Bartnykaitė A, Ugenskienė R and Juozaitytė E. siRNA knockdown of REDD1 facilitates aspirin-mediated dephosphorylation of mTORC1 target 4E-BP1 in MDA-MB-468 human breast cancer cell line. Cancer Manag Res 2021; 13: 1123-1133.
[13] Liao KF, Chiu TL, Huang SY, Hsieh TF, Chang SF, Ruan JW, Chen SP, Pang CY and Chiu SC. Anti-cancer effects of radix angelica sinensis (Danggui) and N-Butylidenephthalide on gastric cancer: implications for REDD1 activation and mTOR inhibition. Cell Physiol Biochem 2018; 48: 2231-2246.
[14] Ben Sahra I, Regazzetti C, Robert G, Laurent K, Le Marchand-Brustel Y, Auberger P, Tanti JF, Giorgetti-Peraldi S and Bost F. Metformin, inde-pendent of AMPK, induces mTOR inhibition and cell-cycle arrest through REDD1. Cancer Res 2011; 71: 4366-4372.
[15] Niu M, Li L, Su Z, Wei L, Pu W, Zhao C, Ding Y, Wazir J, Cao W, Song S, Gao Q and Wang H. An integrative transcriptome study reveals Ddit4/Redd1 as a key regulator of cancer cachexia in rodent models. Cell Death Dis 2021; 12: 652.
[16] DeYoung MP, Horak P, Sofer A, Sgroi D and Ellisen LW. Hypoxia regulates TSC1/2-mTOR signaling and tumor suppression through REDD1-mediated 14-3-3 shuttling. Genes Dev 2008; 22: 239-251.
[17] Mu N, Lei Y, Wang Y, Wang Y, Duan Q, Ma G, Liu X and Su L. Inhibition of SIRT1/2 upregulates HSPA5 acetylation and induces pro-survival autophagy via ATF4-DDIT4-mTORC1 axis in human lung cancer cells. Apoptosis 2019; 24: 798-811.
[18] Gao C, Wang R, Li B, Guo Y, Yin T, Xia Y, Zhang F, Lian K, Liu Y, Wang H, Zhang L, Gao E, Yan W and Tao L. TXNIP/Redd1 signalling and excessive autophagy: a novel mechanism of myocardial ischaemia/reperfusion injury in mice. Cardiovasc Res 2020; 116: 645-657.
[19] Yin H, Wang K, Das A, Li G, Song Y, Luo R, Cheung JPY, Zhang T, Li S and Yang C. The REDD1/TXNIP complex accelerates oxidative stress-induced apoptosis of nucleus pulposus cells through the mitochondrial pathway. Oxid Med Cell Longev 2021; 2021: 7397516.
[20] Liu Q, He H, Yuan Y, Zeng H, Wang Z and Luo W. Novel expression of EGFL7 in osteosarcoma and sensitivity to cisplatin. Front Oncol 2020; 10: 74.
[21] Yuan Y, Liu Q, Wu Z and Luo W. Mechanistic insight on the interaction between OPN and integrin alphanubeta3 in osteoarthritis. Biomed Res Int 2020; 2020: 2905634.
[22] Lin J, Xu Z, Xie J, Deng X, Jiang L, Chen H, Peng C, Li H, Zhang J and Shen B. Oncogene APOL1 promotes proliferation and inhibits apoptosis via activating NOTCH1 signaling pathway in pancreatic cancer. Cell Death Dis 2021; 12: 760.
[23] Villanueva F, Araya H, Briceño P, Varela N, Stevenson A, Jerez S, Tempio F, Chnaiderman J, Perez C, Villarroel M, Concha E, Khani F, Thaler R, Salazar-Onfray F, Stein GS, van Wijnen AJ and Galindo M. The cancer-related transcription factor RUNX2 modulates expression and secretion of the matricellular protein osteopontin in osteosarcoma cells to promote adhesion to endothelial pulmonary cells and lung metastasis. J Cell Physiol 2019; 234: 13659-13679.
[24] Gusho CA, Miller I, Clayton B, Colman MW, Gitelis S and Blank AT. The prognostic significance of lymphovascular tumor invasion in localized high-grade osteosarcoma: outcomes of a single institution over 10 years. J Surg Oncol 2021; 123: 1624-1632.
[25] Shen S, Yao T, Xu Y, Zhang D, Fan S and Ma J. CircECE1 activates energy metabolism in osteosarcoma by stabilizing c-Myc. Mol Cancer 2020; 19: 151.
[26] Vaira S, Friday E, Scott K, Conrad S and Turturro F. Wnt/beta-catenin signaling pathway and thioredoxin-interacting protein (TXNIP) mediate the “glucose sensor” mechanism in metastatic breast cancer-derived cells MDA-MB-231. J Cell Physiol 2012; 227: 578-586.
[27] Chen Q, Liu T, Bao Y, Zhao T, Wang J, Wang H, Wang A, Gan X, Wu Z and Wang L. CircRNA cRAPGEF5 inhibits the growth and metastasis of renal cell carcinoma via the miR-27a-3p/TXNIP pathway. Cancer Lett 2020; 469: 68-77.
[28] Xiao J, Zhu Y, Liu Y, Tipoe GL, Xing F and So KF. Lycium barbarum polysaccharide attenuates alcoholic cellular injury through TXNIP-NLRP3 inflammasome pathway. Int J Biol Macromol 2014; 69: 73-78.
[29] Yoshihara E, Masaki S, Matsuo Y, Chen Z, Tian H and Yodoi J. Thioredoxin/Txnip: redoxisome, as a redox switch for the pathogenesis of diseases. Front Immunol 2014; 4: 514.
[30] Xu Q, Guohui M, Li D, Bai F, Fang J, Zhang G, Xing Y, Zhou J, Guo Y and Kan Y. lncRNA C2dat2 facilitates autophagy and apoptosis via the miR-30d-5p/DDIT4/mTOR axis in cerebral ischemia-reperfusion injury. Aging (Albany NY) 2021; 13: 11315-11335.

[31] Zhang F, Liu G, Li D, Wei C and Hao J. DDIT4 and associated lncDDIT4 modulate Th17 differentiation through the DDIT4/TSC/mTOR pathway. J Immunol 2018; 200: 1618-1626.
[32] Yang B, Xu B, Yang R, Fu J, Li L, Huo D, Chen J, Yang X, Tan C, Chen H and Wang X. Long noncoding antisense RNA DDIT4-AS1 regulates meningitic escherichia coli-induced neuroinflammation by promoting DDIT4 mRNA stability. Mol Neurobiol 2022; 59: 1351-1365.
[33] Horak P, Crawford AR, Vadysirisack DD, Nash ZM, DeYoung MP, Sgroi D and Ellisen LW. Negative feedback control of HIF-1 through REDD1-regulated ROS suppresses tumorigenesis. Proc Natl Acad Sci U S A 2010; 107: 4675-4680.
[34] Fattahi F, Kiani J, Alemrajabi M, Soroush A, Naseri M, Najafi M and Madjd Z. Overexpression of DDIT4 and TPTEP1 are associated with metastasis and advanced stages in colorectal cancer patients: a study utilizing bioinformatics prediction and experimental validation. Cancer Cell Int 2021; 21: 303.
[35] Li Y, Tao L, Zuo Z, Zhou Y, Qian X, Lin Y, Jie H, Liu C, Li Z, Zhang H, Zhang H, Cen X, Yang S and Zhao Y. ZY0511, a novel, potent and selective LSD1 inhibitor, exhibits anticancer activity against solid tumors via the DDIT4/mTOR pathway. Cancer Lett 2019; 454: 179-190.
[36] Chaves AB, Miranda ER, Mey JT, Blackburn BK, Fuller KNZ, Stearns B, Ludlow A, Williamson DL, Houmard JA and Haus JM. Exercise reduces the protein abundance of TXNIP and its interacting partner REDD1 in skeletal muscle: potential role for a PKA-mediated mechanism. J Appl Physiol (1985) 2022; 132: 357-366.
[37] Zhou H, Shen Q, Fu J, Jiang F, Wang L and Wang Y. Analysis of lncRNA UCA1-related downstream pathways and molecules of cisplatin re-sistance in lung adenocarcinoma. J Clin Lab Anal 2020; 34: e23312.
[38] Shibutani S, Okazaki H and Iwata H. Dynamin-dependent amino acid endocytosis activates mechanistic target of rapamycin complex 1 (mTORC1). J Biol Chem 2017; 292: 18052-18061.
[39] Wang Y, Zhang M, Wang Z, Guo W and Yang D. MYC-binding lncRNA EPIC1 promotes AKT-mTORC1 signaling and rapamycin resistance in breast and ovarian cancer. Mol Carcinog 2020; 59: 1188-1198.
[40] Qiao S, Dennis M, Song X, Vadysirisack DD, Salunke D, Nash Z, Yang Z, Liesa M, Yoshioka J, Matsuzawa S, Shirihai OS, Lee RT, Reed JC and Ellisen LW. A REDD1/TXNIP pro-oxidant complex regulates ATG4B activity to control stress-induced autophagy and sustain exercise capacity. Nat Commun 2015; 6: 7014.
[41] Hou X, Yang S and Yin J. Blocking the REDD1/TXNIP axis ameliorates LPS-induced vascular endothelial cell injury through repressing oxidative stress and apoptosis. Am J Physiol Cell Physiol 2019; 316: C104-C110.

Table S1. Primer sequences

Primer name	Primer sequence
TXNIP Forward Sequence	CAGCAGTGCAAACAGACTTCGG
TXNIP Reverse Sequence	CTGAGGAAGCTCAAAGCCGAAC
DDIT4 Forward Sequence	GTTTGACCGCTCCACGAGCCT
DDIT4 Reverse Sequence	GCACACAAGTGTTCATCCTCAGG
GAPDH Forward Sequence	GTCTCCTCTGACTTCAACAGCG
GAPDH Reverse Sequence	ACCACCCTGTTGCTGTAGCCAA